Vortex localization in single crystals of $Tl_2Ba_2CuO_{6+\delta}$ with columnar defects: An empirical model

M. A. R. LeBlanc and Daniel S. M. Cameron
Department of Physics, University of Ottawa, Ottawa, Ontario, Canada K1N 6N5
(Received 9 June 1997)

The peaks and valleys observed by Nowak *et al.* [Phys. Rev. B **54**, R12 725 (1996)] in the local magnetization $M(x)$ and local relaxation rate $S(x)$ in a single crystal of $Tl_2Ba_2CuO_{6+\delta}$ containing columnar defects are well reproduced by an empirical model where the critical current density j_c is fractionally enhanced in the vicinity of the matching field B_ϕ and of a multiple of B_ϕ by superimposing two broad triangular peaks on a continuous dependence of j_c on the magnetic flux density B. The dependence of $S(x)$ on $B(x)$ is well reproduced by stipulating that j_c decays at a rate $\approx \frac{1}{2}$ slower at the summit of the peaks than at their edges. The model fits the variety of $M(x)$ and $S(x)$ data taking B_{s1} and B_{s2}, the flux density at the first and second peaks in j_c, to have a ratio $B_{s2}/B_{s1} \approx 2.5$. The model also makes detailed predictions regarding the structure and location of valleys for $S(x)$ versus $B(x)$ descending in magnitude which were not reported in the above article. [S0163-1829(98)04309-4]

INTRODUCTION

Nowak *et al.*[1] report a richer variety of structures in the dependence of the local magnetization $M(x)$ and local rate of decay $S(x)$ on the local magnetic flux density $B(x)$ below 12 K in single crystals of the anisotropic high-temperature superconductor $Tl_2Ba_2CuO_{6+\delta}$ containing columnar defects than encountered earlier by Beauchamp *et al.*[2,3] in untwinned single crystals of $YBa_2Cu_3O_{7-\delta}$. The latter[2,3] observed a rapid descent in $|M(x)|$ and a dip or notch in $S(x)$ versus $B(x)$ ascending in magnitude in the vicinity of B_ϕ, the matching field where the density of columnar defects corresponds to the flux line density. Peaks and valleys observed by Nowak *et al.*[1] in the graphs of $M(x)$ and $S(x)$ versus $B(x)$ are also clearly linked to the matching field B_ϕ and a multiple of this quantity. Here $\mu_0 M(x) = B(x) - \mu_0 H_a$, where H_a is the applied field.

We present a simple empirical model which successfully reproduces all of the above observations reported by Nowak *et al.*[1] and their relative positions and magnitudes. The model superimposes two peaks on the standard monotonic dependence of the critical current density j_c on the magnetic flux density B. The location, height and width of these peaks in $j_c(B)$ as well as the ''background'' dependence of j_c on B are chosen to generate curves of $M(x)$ versus $B(x)$ which correspond closely to the measured curve when $B(x)$ is ascending in magnitude.[1] We then show that this prescription for j_c versus B generates a curve for $M(x)$ versus $B(x)$ descending in magnitude which displays peaks and valleys whose location and structure closely match that encountered in the corresponding data curves.[1] We stress that these good fits are achieved without introducing discontinuities[3–5] in the dependence of j_c on B.

Next, exploiting a simple approach to describe the relative rate of relaxation of the flux density configurations and introducing a simple structure in the dependence of dj_c/dt on B, we reproduce the observations of Nowak *et al.*[1] for $S(x)$ versus $B(x)$ ascending in magnitude. Our model also generates detailed predictions for the variation of $S(x)$ with $B(x)$ descending in magnitude. In particular, the model predicts that (i) $B_{V1}\downarrow$ and $B_{V2}\downarrow$ the two valleys for $S(x)$ when $B(x)$ is descending in magnitude will occur at higher values of $B(x)$ than $B_{V1}\uparrow$ and $B_{V2}\uparrow$ encountered when $B(x)$ is ascending in magnitude and (ii) the ratio $B_{V2}\downarrow/B_{V1}\downarrow$ will be appreciably smaller than $B_{V2}\uparrow/B_{V1}\uparrow$ where the subscripts 1 and 2 denote the first and second valley.

FRAMEWORK AND RESULTS OF THE MODEL

First we address the hysteresis curves $M(x)$ versus $B(x)$. The dependence of j_c on B which we exploit is displayed in Fig. 1. For simplicity we choose the well known Kim[6] type of expression for the ''background'' curve of j_c versus B

$$j_c = j_0 \left(\frac{B_{\rm ref}}{B + B_0} \right)^n, \tag{1}$$

where we visualize that the temperature-dependent parameters j_0, $B_{\rm ref}$, B_0, and n will vary with the previous heavy ion irradiation.[1–3,7–15] The two peaks in j_c versus B which are superimposed on this background are, for simplicity, chosen to be ''triangular'' with symmetric slopes on the left and right of the summits. Therefore we write

$$j_{C1L}[B(x)] = j_{S1}\left(\frac{B(x) - B_{A1}}{B_{S1} - B_{A1}} \right), \tag{2a}$$

$$j_{C1R} = j_{S1}\left(\frac{B_{B1} - B(x)}{B_{B1} - B_{S1}} \right) \tag{2b}$$

for the left and right sides of the first peak and similarly,

$$j_{C2L}[B(x)] = j_{S2}\left(\frac{B(x) - B_{A2}}{B_{S2} - B_{A2}} \right), \tag{3a}$$

$$j_{C2R} = j_{S2}\left(\frac{B_{B2} - B(x)}{B_{B2} - B_{S2}} \right) \tag{3b}$$

for the second peak. Equations (2) and (3) apply between their respective boundaries $B_{\phi 1L}$, $B_{\phi 1R}$, $B_{\phi 2L}$, and $B_{\phi 2R}$.

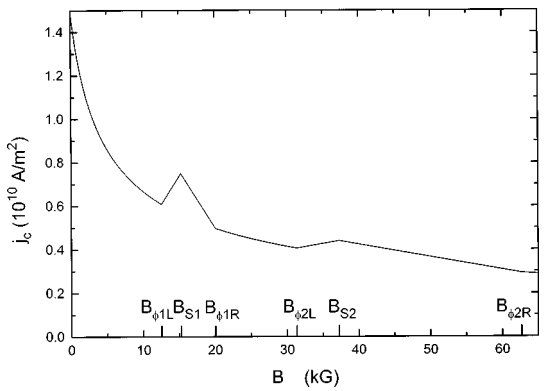

FIG. 1. Display of j_C versus B [Eqs. (1)–(3)] used in our modeling of the pertinent observations (Figs. 1 and 3) of Nowak *et al.*[1] For the ''background'' curve [Eq. (1)] we chose $n=\frac{1}{2}$, $B_0=2.5$ kG, $B_n=(3\mu_0 j_0 X B_{\rm ref}^{1/2}/2)^{2/3}=12.5$ kG and for the triangular peaks we let $B_{\phi 1L}$, B_{S1}, $B_{\phi 1R}$, $B_{\phi 2L}$, B_{S2}, and $B_{\phi 2R}$ equal to 12.5, 15.2, 20, 31.25, 37.14, and 62.5 kG while $j_{S1}=0.75(10^{10})$ A/m^2 and $j_{S2}=0.44(10^{10})$ A/m^2. The parameters were selected to yield a good fit to the curve of $|M(x)|$ versus $B(x)$ ascending in magnitude reported by Nowak *et al.*[1] (see the first and fourth quadrants of their Fig. 1). The model addresses idealized slab or cylinder geometry with $X=R=100$ μm. Triangular peaks were selected for analytic and computational convenience. We note that $B_{S2}/B_{S1}\approx 2.5$.

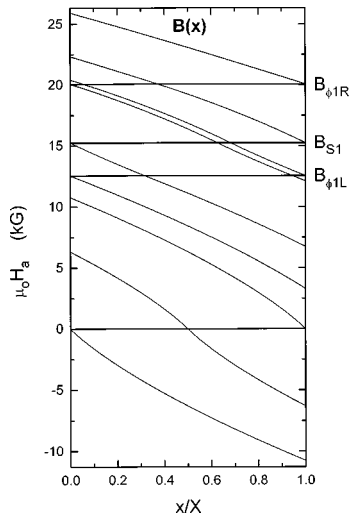

FIG. 2. Displays an illustrative sequence of $B(x)$ profiles generated by $j_C(B)$ of Fig. 1. Here after descending in magnitude from the ''negative'' direction $\mu_0 H_a$ is now ascending in the opposite direction from zero through $B_{\phi 1L}$, B_{S1}, and $B_{\phi 1R}$, hence across the first peak of $j_C(B)$. The surface of the specimen is situated at $x/X=0$ and its center at $x/X=1$. The corresponding $B(x)$ profiles when $\mu_0 H_a$ is descending in magnitude from a large value can be visualized by regarding the surface of the specimen now to be situated at $x/X=1$ and the center at $x/X=0$.

The magnitudes of the critical current densities j_{S1} and j_{S2} at the summit of the two peaks as well as the width of the bases of the peaks and their location are presumably determined by the irradiation which also affects the structure and magnitude of the background curve.[1–3,7–15] In the modeling, the choices for these six quantities dictate the values for B_{A1}, B_{B1}, B_{A2}, and B_{B2}. The various parameters which quantitatively specify j_c versus B displayed in Fig. 1 are selected to yield a good fit to the data reported by Nowak *et al.*,[1] for $M(x)$ versus $B(x)$ ascending in magnitude and are listed in the caption to Fig. 1.

The sequences of critical state profiles of $B(x)$ versus H_a ascending or descending in magnitude are developed from Maxwell's equation $\nabla\times\mathbf{B}=\mu_0\mathbf{j}$, hence, $dB/dx=\pm\mu_0 j_c[B(x)]$ for an idealized slab geometry or $dB/dr=\pm\mu_0 j_c[B(r)]$ for an infinite cylinder. We ignore intrinsic diamagnetism, hence take $B(x)=\mu_0 H(x)$ and the magnetic flux density just inside the surface of the specimen $B_i=\mu_0 H_a$, where H_a is the applied magnetic field.

It is a straightforward albeit tedious exercise to develop detailed expressions for the large variety of critical $B(x)$ profiles which are encountered as the upward and downward sweeps of H_a generate configurations which successively incorporate the detailed structure of j_c versus B displayed in Fig. 1. Some illustrative examples of the sequences of $B(x)$ profiles are displayed in Fig. 2 and in the Appendix. Typical expressions for $B(x)$ versus H_a are developed in the Appendix and a complete set appears in Ref. 16.

Figure 3 displays the results of our calculation of $M(x)$ versus $B(x)$ in a two quadrant format and should be compared with the right half of Fig. 1 of Ref. 1. The peak labeled $P\downarrow$ in Fig. 3 is generated by the ''background'' $j_c(B)$ function [i.e., Eq. (1)] which, although affected by the heavy ion irradiation, is not directly linked to the matching field B_ϕ. This peak is also encountered in the measurements of Beauchamp *et al.*[2,3] The choice of n, $B_{\rm ref}$, and B_0 determine the structure and location of this peak and its magnitude is fixed by the choice of j_0. We note that, in agreement with the observations, the two peaks $P_1\uparrow$ and $P_2\uparrow$ with $|M(x)|$ versus H_a ascending are displaced with respect to the corresponding peaks $P_1\downarrow$ and $P_2\downarrow$, where H_a is descending in magnitude. Thus, the selection for the location of the triangular peaks in j_c versus B in our model (Fig. 1) correctly determines the location of the peaks in $|M(x)|$ versus $B(x)$ descending and ascending in magnitude.

Close examination of Fig. 3 also shows that the four peaks ($P_1\uparrow$, $P_2\uparrow$, $P_1\downarrow$, and $P_2\downarrow$) display asymmetries in agreement with that exhibited by the measured peaks. The asymmetry in the theoretical peaks of $|M(x)|$ versus $B(x)$ arises from the following features in the variation of j_c versus B. The ''background'' j_c [Eq. (1)] is larger on the left of a triangular peak than on its right (see Fig. 1), and, as a consequence the left side of a triangular peak is narrower than its right side although the magnitude of the two slopes are identical. The asymmetry in the humps of $|M(x)|$ versus $B(x)$ is therefore generic in our model and will also appear if exponential, Gaussian, or other centrosymmetric humps for j_c versus B were introduced instead of centrosymmetric triangular peaks.

Decay rates $S(x)$ and $R(x)$ versus $B(x)$. We now examine the rates of local relaxation of the flux density profiles which can be written

$$S(x)=\frac{dB(x)}{dt}=\frac{dB(x)}{dj_0}\frac{dj_0}{dt}=R(x)\frac{dj_0}{dt}, \qquad (4)$$

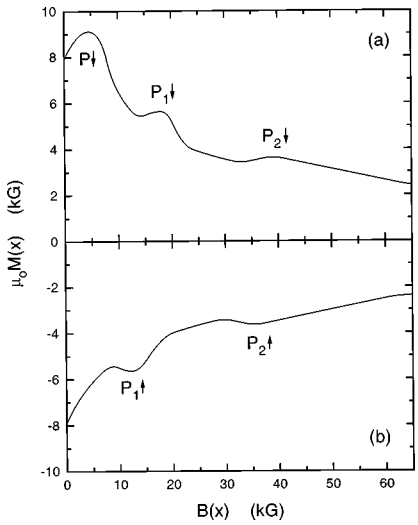

FIG. 3. Displays the local magnetization $\mu_0 M(x) = B(x) - \mu_0 H_a$ versus $B(x)$ which is generated by $j_C(B)$ of Fig. 1 when $B(x)$ is descending (a) and ascending (b) in magnitude. These two calculated curves should be compared with that presented in the right half of Fig. 1 of Nowak *et al.*[1] The height, breadth, and position of the salient features of these curves are modified when the location x/X of the measuring probe is changed. In particular, the position of the summits of the peaks $P_1\downarrow$ and $P_1\uparrow$ approach B_{S1} while $P_2\downarrow$ and $P_2\uparrow$ approach B_{S2} as the location of the measuring probe x/X is moved closer to the surface of the specimen. However, this also causes $|M(x)|$ to diminish. The reason for this emerges from careful examination of representative $B(x)$ profiles shown in Fig. 2. In these calculations $x/X = 2/3$ since this corresponds to the position of the field probe in the measurements reported by Nowak *et al.*[1] Ideally in Fig. 1 of Nowak *et al.*,[1] the curve in the first (fourth) quadrant should be the exact image of that in the third (second) quadrant.

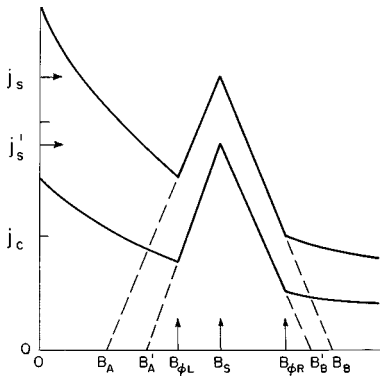

FIG. 4. Schematically illustrates the decay of the critical current density introduced in our model. We visualize that during the decay, the location on the B axis of the boundaries ($B_{\phi 1L}$, $B_{\phi 1R}$, $B_{\phi 2L}$, and $B_{\phi 2R}$) and of the summits (B_{S1} and B_{S2}) of the triangular peaks (only one shown) remains fixed. The rate of decay of the critical current density $j_C(B)$ is assumed independent of the flux density for the background curve [Eq. (1)] but to vary smoothly at the boundaries and linearly along the slopes of the triangular peaks. Good agreement with the data displayed in Fig. 3 of Nowak *et al.*[1] is obtained letting the rate of decay $\Delta j_{S1}/j_{S1}$ and $\Delta j_{S2}/j_{S2}$, at the summits of the triangular peaks to be $\approx \frac{1}{2}\Delta j_0/j_0$, hence $\frac{1}{2}$ the decay rate at the boundaries of the peaks, and to vary linearly along the slopes of the triangular peaks. Initially, for simplicity, we take the triangular peaks to be centrosymmetric, hence, let $B_{S1} = (B_{A1} + B_{B1})/2$ and $B_{S2} = (B_{A2} + B_{B2})/2$. As j_C decays with the location of the boundaries and summit of the triangular peaks remaining fixed, the bases of the triangles B_{A1}, B_{B1}, B_{A2}, and B_{B2} [see Eqs. (2) and (3)] migrate to new values, denoted B'_{A1}, B'_{B1}, B'_{A2}, and B'_{B2}. Also, the left slope of a triangular peak becomes steeper than that on its right, hence now $B_{S1} \neq (B'_{A1} + B'_{B1})/2$ and $B_{S2} \neq (B'_{A2} + B'_{B2})/2$. The continuity of $j_C(B)$ at the boundaries [Eqs. (1)–(3)] yield 0.933, 29.54, −33.188, and 113.08 kG for B_{A1}, B_{B1}, B_{A2}, and B_{B2}. For clarity, the amount of decay of $j_C(B)$ is greatly exaggerated in the figure.

where it is assumed that dj_0/dt does not depend on $B(x)$. We focus on the relative rate $R(x) = dB(x)/(dj_0/j_0)$ and on the normalized rate $R_n(x) = dB(x)/[\mu_0 M(x) dj_0/j_0]$.

Our treatment is a simple extension of an approach already exploited by several workers.[5,17–20] In this framework the decay of the critical state configuration is determined by the decrease of the current density parameters j_0, j_{S1}, and j_{S2} in Eqs. (1), (2), and (3). As the parameter j_0 of the background curve [Eq. (1)] decreases by an amount Δj_0 we visualize that $j_c(B)$ along the triangular summits decays as illustrated schematically in Fig. 4. The diminution of j_c at the summits can be written

$$\frac{\Delta j_{S1}}{j_{S1}} = f_1 \frac{\Delta j_0}{j_0}$$

and

$$\frac{\Delta j_{S2}}{j_{S2}} = f_2 \frac{\Delta j_0}{j_0}. \tag{5}$$

We obtain good agreement with the pertinent data of Nowak *et al.*[1] by letting $f_1 = f_2 = \frac{1}{2}$. We assume, for simplicity, that the rate of decay of $j_C(B)$ along the slopes of the triangular summits varies linearly versus $B(x)$ from its value at the junctions with the background curve (i.e., the boundaries $B_{\phi 1L}$, $B_{\phi 1R}$, $B_{\phi 2L}$, and $B_{\phi 2R}$) to a smaller value at the summits B_{S1} and B_{S2}. (i) The continuity of $j_C(B)$ at the boundaries and (ii) the constraint that the location of these boundaries as well as the location of the summits along the B axis remain fixed, as j_0, j_{S1}, and j_{S2} diminish, dictate the evolution of B_{A1}, B_{B1}, B_{A2}, and B_{B2} in Eqs. (2) and (3), hence determine the relaxation of the flux density profiles. The results of this exercise are displayed in Figs. 5 and 6 where for completeness and clarity we present both R_n and R, the normalized and unnormalized relative relaxation rates for $B(x)$ increasing and decreasing in magnitude. We note, however, that the normalized relaxation rate, a composite quantity of two ingredients, has the drawback that it contains the experimental errors or modeling approximations of the two constituents.

Figure 5(a) is seen to reproduce the major features of the pertinent observations of Nowak *et al.*[1] (see their Fig. 3). The fact that $B_{V1}\uparrow$ and $B_{V2}\uparrow$, the location of the bottom of the two valleys, corresponds to that encountered by Nowak *et al.*,[1] hence closely match B_ϕ and $3B_\phi$, ensues from our choices for the parameters $B_{\phi 1L}$, $B_{\phi 1R}$, j_{S1}, $B_{\phi 2L}$, $B_{\phi 2R}$, and j_{S2}, which were selected to account for the location, magnitude and structure of the peaks ($P_1\uparrow$, $P_2\uparrow$, $P_1\downarrow$, and

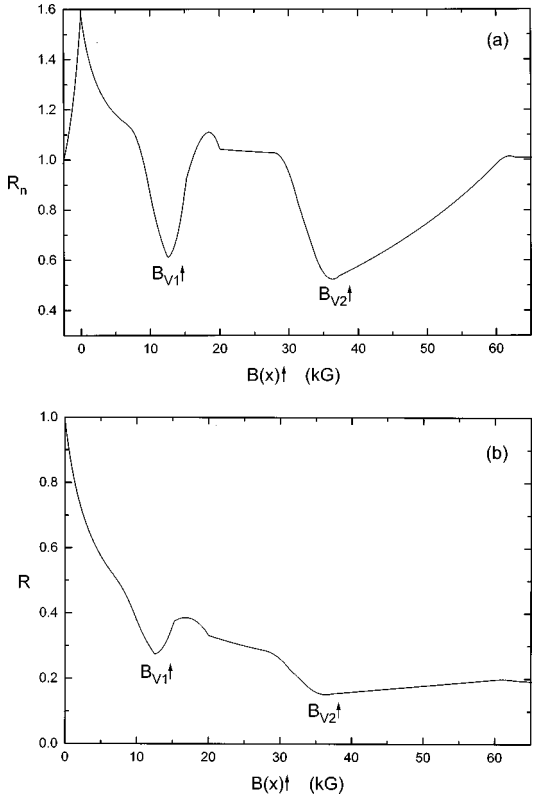

FIG. 5. (a) displays the normalized initial relaxation rate $R_n = |\Delta B(x)/\mu_0 M(x)(\Delta j_0/j_0)|$ versus $B(x)$ calculated for $x/X = \frac{2}{3}$ using the decay of $j_C(B)$ schematically illustrated in Fig. 4. Here $B(x)$ after descending in magnitude through zero is ascending in magnitude in the opposite direction (see Fig. 1 of Nowak *et al.*[1]). This ''theoretical'' curve should be compared with the curve traced by the open circle data of Fig. 3 of Nowak *et al.*[1] The salient features of the structure of the theoretical curve persist but absolute and relative values of $M(x)$ change with the location of the measuring probe. In particular, the position of the minima $B_{V1}\uparrow$ and $B_{V2}\uparrow$ approach B_{S1} and B_{S2}, hence the ratio $B_{V2}\uparrow/B_{V1}\uparrow$ approaches $B_{S2}/B_{S1} \approx 2.5$ from above as the probe is placed closer to the surface of the specimen. Careful consideration of Figs. 2 and 4 indicate why this occurs with our model. (b) complements (a) by displaying the corresponding initial relaxation rate $R = |\Delta B(x)/B_n(\Delta j_0/j_0)|$ versus $B(x)$, hence here the separately calculated (and measured) quantity $M(x)$ is not introduced. For convenience, however, $B(x)$ is normalized with respect to the parameter $B_n = (3\mu_0 j_0 X B_{\rm ref}^{1/2}/2)^{2/3}$. When $B(x) = 0$, $R = (2/3)(x/X)/(B_0/B_n)^{1/2}$ (see the Appendix), hence the feature that here $R(0) \approx 1.0$ is coincidental and a consequence of our choices for x/X and B_0/B_n.

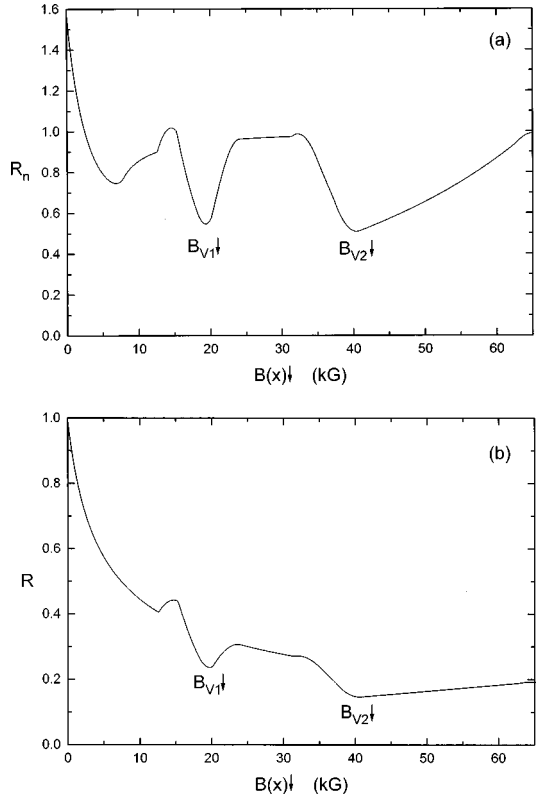

FIG. 6. Complements Fig. 5 by displaying the corresponding ''predicted'' initial relaxation rates R_n and R where now $B(x)$ is descending in magnitude from a large value. Nowak *et al.*[1] do not report on the relaxation rate under these circumstances. Comparing these curves with the corresponding curves of Fig. 5 we note that the model predicts that, for any chosen location of the measuring probe, $B_{V1}\downarrow > B_{V1}\uparrow$, $B_{V2}\downarrow > B_{V2}\uparrow$ and $B_{V2}\downarrow/B_{V1}\downarrow < B_{V2}\uparrow/B_{V1}\uparrow$. Further $B_{V1}\downarrow$ and $B_{V2}\downarrow$ approach B_{S1} and B_{S2} hence the ratio $B_{V2}\uparrow/B_{V1}\uparrow$ approaches $B_{S2}/B_{S1} \approx 2.5$ from below as the probe is placed closer to the surface of the specimen. Again, careful consideration of Figs. 2 and 4 indicates that these results are generic features of our model hence do not depend on our choice of a triangular structure for the peaks in $j_C(B)$ and our simple prescription for the ''background'' decrease of j_C versus B.

$P_2\downarrow$) in the local hysteresis curves. The depths of the valleys relative to their shoulders is mainly controlled by the choices for f_1 and f_2. Asymmetry in the structure of the valleys arises from the same feature that causes the asymmetry of the peaks in Fig. 3; namely, that $(B_{\phi 1R} - B_{S1}) > (B_{S1} - B_{\phi 1L})$ and $(B_{\phi 2R} - B_{S2}) > (B_{S2} - B_{\phi 2L})$ for the centrosymmetric triangular peaks (see Figs. 1 and 4).

In our model, the peak straddling $B(x) = 0$ arises from the large j_C at low fields and its strong dependence on magnetic flux density.[5] The latter properties are produced by the heavy ion irradiation.[2,7–15] The feature that the measured peak is not centered at $B(x) = 0$ may be due to the large demagnetization factor encountered with the platelet specimens in the experiments.

The model generates detailed predictions regarding the evolution of (i) the position along the $B(x)$ axis of the bottom of the valleys and (ii) the structure of these valleys as a function of the location x/X of the measuring probes. We note that $B_{V1}\uparrow$ and $B_{V2}\uparrow$, the location of the bottom of the valleys along the $B(x)$ axis occurs at slightly lower fields than B_{S1} and B_{S2}, the summits of the triangular peaks in j_C versus B. In our model, the values of the former depends on the location of the measuring probe (see the Appendix). Here $B_{V2}\uparrow/B_{V1}\uparrow \approx 2.8$ whereas $B_{S2}/B_{S1} \approx 2.5$ (see Fig. 1).

The ''acid test'' of the predictive value of the model, however, resides mainly in the curves it generates for R and R_n [hence $S(x)$ and $S_n(x)$] versus $B(x)$ descending in magnitude. These predictions are displayed in Fig. 6. The first low field valley appearing in the graph of $R_n(x)$ versus $B(x)$ descending in magnitude is, in a sense, an artifact of the

normalization with respect to $|M(x)|$ since the latter traces a pronounced peak in this range of $B(x)$ [see the upper curve of Fig. 3 and Fig. 6(b)]. We note that $B_{V1}\downarrow$ and $B_{V2}\downarrow$, the bottoms of the valleys when $B(x)$ is descending in magnitude appear at significantly higher fields than B_{S1} and B_{S2}, the summits of the triangular peaks in $j_C(B)$. An important related consequence is that the ratio $B_{V2}\downarrow/B_{V1}\downarrow\approx 2$ is appreciably smaller than the ratio $B_{S2}/B_{S1}\approx 2.5$. Again, we stress that in our model $B_{V1}\downarrow$, $B_{V2}\downarrow$, and their ratio depend on the location of the measuring probe.

SUMMARY AND CONCLUSION

We have developed an empirical model which semiquantitatively accounts for the location and structure of peaks in the local magnetization $|M(x)|$ and a central peak and valleys in the local relaxation rate $R_n(x)$ versus $B(x)$ observed by Nowak *et al.*[1] in a single crystal of an anisotropic high-T_C superconductor containing columnar defects. In agreement with observations, the location of the peaks and valleys and their structure depend on (i) whether $B(x)$ is ascending or descending in magnitude and (ii) the position of the measuring probes. As a consequence the ratios for the values observed for various salient features (namely, $B_{P2}\uparrow/B_{P1}\uparrow$, $B_{P2}\downarrow/B_{P1}\downarrow$, $B_{V2}\uparrow/B_{V1}\uparrow$, and $B_{V2}\downarrow/B_{V1}\downarrow$) all depend on (i) and (ii). These are generic features of the model although the detailed variations are dependent on the prescription selected for the background curve and the structure of the peaks of $j_C(B)$.

The model visualizes that after heavy ion irradiation the critical current density $j_C(B)$ remains a continuous function of the flux density but rises steeply in the low field range and now exhibits peaks whose summits situated at B_{S1} and B_{S2} on the B axis are linked to the matching field B_ϕ.[1,21–25] For convenience we introduced centrosymmetric triangular peaks instead of more realistic exponential or Gaussian peaks. Presumably the width and height of these two peaks is influenced by the random distribution of the columnar defects and an ordered lattice of defects would give rise to higher and narrower peaks.

To reproduce the observed valleys in the relaxation rate versus $B(x)$ we introduce a simple variation of the decay rate along the slopes of the triangular peaks of $j_C(B)$ where the decay rate is smaller by a factor of $\approx\frac{1}{2}$ at the summits relative to that along their bases. For convenience and in good agreement with observations this factor is chosen the same for both summits. We may conjecture that for a perfectly ordered lattice of columnar defects the decay rate of j_C at the center of the peaks might approach zero.

Our approach provides a good estimate of the dependence of j_C and of its decay rate on the magnetic flux density from the measurements of $M(x)$ and $S(x)$ versus $B(x)$ of Nowak *et al.*[1] and makes detailed predictions regarding the unreported curve of $S(x)$ versus $B(x)$ descending in magnitude. A good fit to the measured curves is obtained by taking the ''summit'' ratio $B_{S2}/B_{S1}\approx 2.45$ in the curve of j_C versus B. This is seen to generate the observed ''valley'' ratio $B_{V2}(x)\uparrow/B_{V1}(x)\uparrow\approx 3$. Future applications of first principle models[26,27] will hopefully account for the appearance of the peaks in the structure of j_C versus B, the variation of the decay rate of j_C along these peaks and the correspondence of these features with B_ϕ and multiples of B_ϕ. Consequently these theoretical efforts should shed light on the physical origin of the ratio $B_{S2}/B_{S1}\approx 2.5$ which emerges from our analysis of the observations of Nowak *et al.*[1]

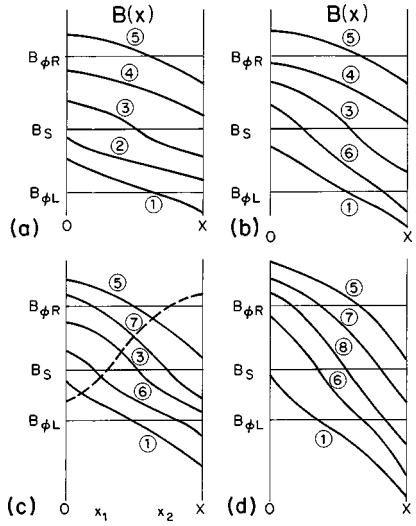

FIG. 7. Illustrates the four scenarios in the sequences of $B(x)$ profiles which can be encountered as $\mu_0 H_a$ ascending or descending in magnitude generates $B(x)$ profiles traversing a peak in $j_C(B)$. We note that the location of the measuring probe as well as the ''structure'' of $j_C(B)$ (Fig. 1) prescribing the $B(x)$ profiles determine which scenario is encountered.

APPENDIX

Calculation of $B(x)$ profiles. In our framework, where $j_C(B)$ exhibits a peak or peaks, four scenarios for the sequences of configurations of flux density profiles (and their ''images'') need to be envisaged as an increase (decrease) of the magnitude of the applied field H_a induces field shielding (flux retaining) critical current densities in the specimen. These four scenarios are displayed schematically in Fig. 7. These sketches show the sequences of B profiles for H_a ascending (descending) in magnitude if we regard the surface and the center of a specimen of idealized planar geometry to be situated at $x=0$ and $x=X$ ($x=X$ and $x=0$). Note the appearance of a profile labeled 6 (7,8) and the absence of that labeled 2 (4,3) in Fig. 7(b) [7(c), 7(d)].

To illustrate the calculation of these sequences of $B(x)$ profiles for $j_C(B)$ displayed in Fig. 1 we focus on a representative case, namely, that labeled 7 in Fig. 7(c). To fix ideas we consider that this profile pertains to the first triangular peak in $j_C(B)$.

For idealized planar geometry, the Maxwell equation $\nabla\times\mathbf{B}=\mu_0\mathbf{j}$, together with the critical state assumption that $j=j_C(B)$, reads

$$\frac{dB}{dx}=\pm\mu_0 j_c(B). \tag{A1}$$

First we consider $B(x)$ ascending in magnitude. For the region $0\leqslant x\leqslant x_1$, where j_C is given by $j_C=j_0 B_{\rm ref}^n/(B+B_0)^n$ [Eq. (1)], integration of Eq. (A1) leads to

$$B(x)=\{(B_i+B_0)^{n+1}-\mu_0(n+1)j_0B_{\rm ref}^n x\}^{1/(n+1)}-B_0, \tag{A2}$$

where $B_i=\mu_0 H_a$ is the flux density just inside the surface.

Letting $B(x_1)=B_{\phi 1R}$ gives

$$x_1=\frac{(B_i+B_0)^{n+1}-(B_{\phi 1R}+B_0)^{n+1}}{\mu_0(n+1)j_0B_{\rm ref}^n}. \tag{A3}$$

For the region $x_1\leqslant x\leqslant x_2$, where $j_C=J_{C1R}=j_{S1}\{B_{B1}-B(x)\}/\{B_{B1}-B_{S1}\}$ [Eq. 2(b)], integration of Eq. (A1) leads to

$$B(x)=B_{B1}-(B_{B1}-B_{\phi 1R})e^{\mu_0 j_{S1}(x-x_1)/(B_{B1}-B_{S1})}. \tag{A4}$$

Letting $B(x_2)=B_{S1}$, gives

$$x_2=\frac{(B_{B1}-B_{S1})}{\mu_0 j_{S1}}\ln\left\{\frac{B_{B1}-B_{S1}}{B_{B1}-B_{\phi 1R}}\right\}+x_1, \tag{A5}$$

where x_1 is given by Eq. (A3).

For the region $x_2\leqslant x\leqslant X$, where $j_C=j_{C1L}=j_{S1}\{B(x)-B_{A1}\}/\{B_{S1}-B_{A1}\}$ [Eq. (2a)], integration of Eq. (A1) leads to

$$B(x)=B_{A1}+(B_{S1}-B_{A1})e^{-\mu_0 j_{S1}(x-x_2)/(B_{S1}-B_{A1})}, \tag{A6}$$

where x_2 is given by Eq. (A5).

For H_a descending in magnitude we focus on the $B(x)$ profile shown by the dashed curve, also labeled 7 in Fig. 7(c). The procedure already outlined leads to

$$B(x)=B_{A1}+(B_i-B_{A1})e^{\mu_0 j_{S1}x/(B_{S1}-B_{A1})} \tag{A7}$$

valid for $0\leqslant x\leqslant x_1$, where

$$x_1=\frac{(B_{S1}-B_{A1})}{\mu_0 j_{S1}}\ln\left\{\frac{B_{S1}-B_{A1}}{B_i-B_{A1}}\right\} \tag{A8}$$

and

$$B(x)=B_{B1}-(B_{B1}-B_{S1})e^{-\mu_0 j_{S1}(x-x_1)/(B_{B1}-B_{S1})} \tag{A9}$$

valid for $x_1\leqslant x\leqslant x_2$, where x_2 is given by Eq. (A5) but where x_1 is now given by Eq. (A8). Also,

$$B(x)=\{(B_{\phi 1R}+B_0)^{n+1}+\mu_0(n+1)j_0B_{\rm ref}^n x-x_2\}^{1/(n+1)}-B_0 \tag{A10}$$

valid for $x_2\leqslant x\leqslant X$.

The parameters which determine the ''background'' $j_C(B)$ [Eq. (1)], namely, j_0, $B_{\rm ref}$, B_0, and n are selected to provide a satisfactory description of the observed ''background'' curve for $|M(x)|$ versus $B(x)$ ascending or descending. The parameters which determine the location, width and height of the triangular peaks in $j_c(B)$, hence $B_{\phi 1L}$, $B_{\phi 1R}$, j_{S1}, $B_{\phi 2L}$, $B_{\phi 2R}$, and j_{S2} are selected to give a good description of the peaks observed for $|M(x)|$ versus $B(x)$ ascending or descending in magnitude.

The requirement that $j_c(B)$ be continuous is met by the conditions that

$$j_C(B_{\phi 1L})=j_0\left(\frac{B_{\rm ref}}{B_{\phi 1L}+B_0}\right)^n=j_{C1L}=j_{S1}\left(\frac{B_{\phi 1L}-B_{A1}}{B_{S1}-B_{A1}}\right), \tag{A11}$$

$$j_C(B_{\phi 1R})=j_0\left(\frac{B_{\rm ref}}{B_{\phi 1R}+B_0}\right)^n=j_{C1R}=j_{S1}\left(\frac{B_{B1}-B_{\phi 1R}}{B_{B1}-B_{S1}}\right) \tag{A12}$$

which prescribe the parameters B_{A1} and B_{B1}, and the similar conditions

$$j_C(B_{\phi 2L})=j_0\left(\frac{B_{\rm ref}}{B_{\phi 2L}+B_0}\right)^n=j_{C2L}=j_{S1}\left(\frac{B_{\phi 2L}-B_{A2}}{B_{S2}-B_{A2}}\right), \tag{A13}$$

$$j_C(B_{\phi 2R})=j_0\left(\frac{B_{\rm ref}}{B_{\phi 2R}+B_0}\right)^n=j_{C2R}=j_{S2}\left(\frac{B_{B2}-B_{\phi 2R}}{B_{B2}-B_{S2}}\right) \tag{A14}$$

which dictate the parameters B_{A2} and B_{B2}. In order that the triangular peaks be centrosymmetric we write

$$B_{S1}=(B_{A1}+B_{B1})/2$$

and

$$B_{S2}=(B_{A2}+B_B)/2. \tag{A15}$$

Calculation of relaxation rate $R(x)$. The local relative relaxation rate $R(x)$ is calculated by letting the critical current density parameters j_0, j_{S1}, and j_{S2} decay to $j_0'=j_0-\Delta j_0$, $j_{S1}'=j_{S1}-\Delta j_{S1}$, and $j_{S2}'=j_{S2}-\Delta j_{S2}$ in the expression for the $B(x)$ profiles. To generate differences in decay rates for $j_c(B)$ along the triangular peaks relative to that prevailing along the background curve we write

$$\frac{\Delta j_{S1}}{j_{S1}}=f_1\frac{\Delta j_0}{j_0}$$

and

$$\frac{\Delta j_{S2}}{j_{S2}}=f_2\frac{\Delta j_0}{j_0}. \tag{A16}$$

We also stipulate that (i) $j_c(B)$ remains continuous as it decays, and (ii) the boundaries $B_{\phi 1L}$, $B_{\phi 1R}$, $B_{\phi 2L}$, and $B_{\phi 2R}$ as well as the position of the peak centers B_{S1} and B_{S2}, all remain fixed as illustrated in Fig. 4. These conditions then dictate that the relative decay rate of j_c vary linearly versus B along the slopes of the triangular peaks. Stipulations (i) and (ii) prescribe the evolution of the parameters B_{A1}, B_{B1}, B_{A2}, and B_{B2} to a new set denoted B_{A1}', B_{B1}', B_{A2}', and B_{B2}' via Eqs. (A11)–(A16). We note that the triangular peaks do not remain centrosymmetric as $j_c(B)$ decays since the slope on their left becomes steeper than that on their right (see Fig. 4). This feature of our model will, however, play a role only after appreciable decay has occurred. For the calculations displayed in Figs. 4 and 5 we have focused only on the initial decay rate.

Introducing j_0, j_{S1}, and j_{S2} and the corresponding set of parameters B'_{A1}, B'_{B1}, B'_{A2}, and B'_{B2} into the expressions for $B(x)$ [viz. Eqs. (A2)–(A10)] for the profile under scrutiny we then calculate

$$R(x)=\left|\frac{B_f(x)-B(x)}{B_n(\Delta j_0/j_0)}\right|$$

and

$$R_n(x)=R(x)/|\mu_0 M(x)|/B_n$$

for various selected locations of the flux density sensor in the specimen. Here $B_f(x)$ denotes the infinitesimally relaxed profiles. We note that our results also pertain to infinite cylinder geometry by substituting $(R-r)/R$ for x/X in the expressions for the sequences of $B(x)$ profiles.

[1] E. R. Nowak, S. Anders, H. M. Jaeger, J. A. Fendrich, W. K. Kwok, R. Mogilevsky, and D. G. Hinks, Phys. Rev. B **54**, R12 725 (1996).

[2] K. M. Beauchamp, T. F. Rosenbaum, U. Welp, G. W. Crabtree, and V. M. Vinokur, Phys. Rev. Lett. **75**, 3942 (1995).

[3] K. M. Beauchamp, L. Radzihovsky, E. Shung, T. F. Rosenbaum, U. Welp, and G. W. Crabtree, Phys. Rev. B **52**, 13 025 (1995).

[4] L. Radzihovsky, Phys. Rev. Lett. **74**, 4919 (1995).

[5] M. A. R. LeBlanc, Daniel S. M. Cameron, and David LeBlanc, Phys. Rev. B **55**, R6141 (1997).

[6] Y. B. Kim, C. F. Hempstead, and A. R. Strnad, Phys. Rev. Lett. **9**, 306 (1962); Phys. Rev. **129**, 528 (1963); **131**, 2486 (1963).

[7] L. Civale, A. D. Marwick, T. K. Worthington, M. A. Kirk, J. R. Thompson, L. Krusin-Elbaum, Y. Sun, J. R. Clem, and F. Holtzberg, Phys. Rev. Lett. **67**, 648 (1991).

[8] W. Gerhauser, G. Ries, H. W. Neumuller, W. Schmidt, O. Eibl, G. Saemann-Ischenko, and S. Klaumunzer, Phys. Rev. Lett. **68**, 879 (1992).

[9] R. C. Budhani, M. Suenaga, and S. H. Liou, Phys. Rev. Lett. **69**, 3816 (1992).

[10] L. Krusin-Elbaum, L. Civale, J. R. Thompson, and C. Feild, Phys. Rev. B **53**, 11 744 (1996).

[11] M. Konczykowski, F. Rullier-Albenque, E. R. Yacoby, A. Shaulov, Y. Yeshurun, and P. Lejay, Phys. Rev. B **44**, 7167 (1991).

[12] M. Konczykowski, V. M. Vinokur, F. Rullier-Albenque, Y. Yeshurun, and F. Holtzberg, Phys. Rev. B **47**, 5531 (1993).

[13] M. Konczykowski, D. Majer, E. Zeldov, N. Chikumoto, and V. M. Vinokur, Physica C **235–240**, 2965 (1994).

[14] M. Konczykowski, N. Chikumoto, V. M. Vinokur, and M. V. Feigelman, Phys. Rev. B **51**, 3957 (1995).

[15] C. J. van der Beek, M. Konczykowski, V. M. Vinokur, G. W. Crabtree, T. W. Li, and P. H. Kes, Phys. Rev. B **51**, 15 492 (1995).

[16] Daniel S. M. Cameron, M.Sc. Thesis, University of Ottawa, Ottawa, Ontario, Canada, 1997.

[17] Y. Yeshurun, A. P. Malozemoff, F. Holtzberg, and T. R. Dinger, Phys. Rev. B **38**, 11 828 (1988).

[18] Donglu Shi, Ming Xu, A. Umezawa, and Ronald F. Fox, Phys. Rev. B **42**, 2062 (1990).

[19] Ming Xu, Donglu Shi, A. Umezawa, K. G. Vanderwoort, and G. W. Crabtree, Phys. Rev. B **43**, 13 049 (1991).

[20] Yang Ren Sun, J. R. Thompson, D. K. Christen, F. Holtzberg, A. D. Marwick, and J. G. Ossendon, Physica C **194**, 403 (1992).

[21] A. N. Lykov, Solid State Commun. **86**, 531 (1993).

[22] V. V. Metlushko, M. Baert, R. Jonckheere, V. V. Moshchalkov, and Y. Bruynseraede, Solid State Commun. **91**, 331 (1994).

[23] M. Baert, V. V. Metlushko, R. Jonckheere, V. V. Moshchalkov, and Y. Bruynseraede, Phys. Rev. Lett. **74**, 3269 (1995).

[24] V. V. Moshchalkov, M. Baert, V. V. Metlushko, E. Rosseel, M. J. Van Bael, K. Temst, R. Jonckheere, and Y. Bruynseraede, Phys. Rev. B **54**, 7385 (1996).

[25] K. Harada, O. Kamimura, H. Kasai, T. Matsuda, A. Tonomura, and V. V. Moshchalkov, Science **274**, 1167 (1996).

[26] C. Reichhardt, C. J. Olson, J. Groth, Stuart Field, and Franco Nori, Phys. Rev. B **53**, R8898 (1996).

[27] C. Reichhardt, C. J. Olson, and Franco Nori, Phys. Rev. Lett. **78**, 2648 (1997).